Mapping licit and illicit mining activity in the Madre de Dios region of Peru

Arthur Elmes, Josué Gabriel Yarlequé Ipanaqué, John Rogan, Nicholas Cuba & Anthony Bebbington

Published online: 20 Oct 2014.

Submit your article to this journal ⬈

Article views: 191

View related articles ⬈

View Crossmark data ⬈

Taylor & Francis
Taylor & Francis Group

Mapping licit and illicit mining activity in the Madre de Dios region of Peru

Arthur Elmes*, Josué Gabriel Yarlequé Ipanaqué, John Rogan, Nicholas Cuba, and Anthony Bebbington

Graduate School of Geography, Clark University, Worcester, MA 01610, USA

Since the early 2000s, the Madre de Dios Region of southern Peru has experienced rapid expansion of both licit and illicit mining activities, in the form of artisanal and small-scale mining (ASM). ASM typically takes place in remote, inaccessible locations and is therefore difficult to monitor *in situ*. This paper explores the utility of Landsat-5 imagery via decision tree classification to determine ASM locations in Madre de Dios. Spectral mixture analysis was used to unmix Landsat imagery, using WorldView and QuickBird l imagery to aid spectral endmember selection and validate AMS maps. The ASM maps had an overall area-weighted accuracy of 96% and indicated a large proportion of illicit ASM activity (~65% of all ASM in the study area) occurring outside the permitted concessions. Holistic visual comparison of ASM output maps with reference imagery showed that these methods produce reasonable, realistic maps of mined area extent.

1. Introduction

This paper examines the use of Spectral Mixture Analysis (SMA) and Classification Tree Analysis (CTA) of Landsat-5 imagery to map licit and illicit mineral extraction activity, primarily for gold, in the Madre de Dios Department of Peru. Peru is the sixth largest producer of gold worldwide with a 7.68% market share (Vásquez Cordano and Balistreri 2010), with 20% of Peru's gold bullion originating from illicit artisanal and small-scale mining (ASM) (Gardner 2012). The Department of Madre de Dios, with an area of approximately 85,000 km^2, generates roughly 70% of Peru's ASM gold production, although the illicit nature of the mining prevents definitive estimates (Brooks et al. 2007). Both licit and illicit ASM operations result in forest loss and degradation, water and soil mercury contamination, river siltation and mercury-contaminated fish stocks (Hentschel, Hruschka, and Priester 2002; Veiga, Maxson, and Hylander 2006; Yard et al. 2012). Additionally, Asner et al. (2010) noted how ASM-caused forest degradation contributes significantly to carbon storage loss in the Peruvian Amazon. Furthermore, since small-scale illicit mining is inherently illegal, it cannot be mapped or monitored via traditional regulatory/concession documentation, and therefore there is no reliable estimate of the number of illicit mines in Peru (Swenson et al. 2011). Although the historical extent of ASM in Peru has largely been unknown (Mosquera, Chávez, and Pachas 2009), recent research has shown that Landsat data, together with spectral unmixing, can reliably detect ASM locations (Asner et al. 2013). However, to date these SMA methods have not been augmented with ancillary GIS data-sets and decision tree analysis, nor have mapped ASM extents been measured within and outside of legal mining concession boundaries. As global demand for gold continues to increase, so too does the need for effective

---

*Corresponding author. Email: aelmes@clarku.edu

ASM monitoring methods, especially in locations where no regulatory information is available (Hilson 2002, 2005; Bebbington et al. 2008). The goal of this paper is to develop methods for use with freely available Landsat imagery, Advanced Spaceborne Thermal Emission and Reflection Radiometer (ASTER) elevation data and ancillary GIS data, to identify ASM mining operations and to quantify the extent of licit versus illicit ASM in Madre de Dios.

Few studies have quantified the extent and magnitude of surface mining activities associated with ASM, as there has been more focus on larger-scale, industrialized mining (e.g. Latifovic et al. 2005; Slonecker et al. 2010; Erener 2011). For example, Latifovic et al. (2005) used post-classification change detection of Landsat-5 Thematic Mapper (TM) and Lansat-7 Enhanced Thematic Mapper Plus (ETM+) imagery to track decreasing trends in vegetation productivity related to land change caused by oil sand processing in the Athabasca oil sands region in Canada. Baynard (2011) and Baynard, Ellis, and Davis (2013) addressed direct and indirect landscape effects of petroleum exploration and extraction activities in tropical South America, using a combination of Landsat TM/ETM+ imagery and GIS data to create Landscape Infrastructure Footprints. This work highlights the importance of infrastructure development (e.g. roads, clearings, tailing piles, parking zones) and regulation as an explanatory variable for predicting landscape fragmentation and degradation in a mining context. Swenson et al. (2011) used Landsat-5 TM imagery (2003–2009) to map deforestation in the Department of Madre de Dios, indicating that in this time period approximately 6600 ha of primary tropical forest and wetlands were converted to mine-related ponds and tailings. The rate of forest conversion was shown to increase six-fold from 2003–2006 to 2006–2009, and it was linked to an annual increase in global gold prices during the period (Swenson et al. 2011).

While research in remote sensing of illicit mining has been promising, the principal challenge lies in detection of the small, remote and intentionally clandestine patches of disturbance typical of ASM, using moderate spatial resolution (~30 m) imagery (Asner et al. 2013). While several large-scale mining areas exist in the study area (Figure 1) on the order of 100 km^2, ASM operations often occur on scales of tens of km^2, meaning that many ASM sites may go undetected using conventional hard-classification methods. It is important to monitor the proliferation of these smaller ASM locations, since they are contributing to the rapid fragmentation of the region's forest cover (Southworth et al. 2011; Swenson et al. 2011; Asner et al. 2013). The larger and more permanent mining operations, known as Huepetuhe, Guacamayo and Delta-1, are easily captured by moderate spatial resolution data and commonly used classification methods, such as maximum likelihood classification. Conversely, the smaller, distributed nature of much ASM in Madre de Dios results in predominantly mixed pixels, making detection difficult or impossible with such methods. By spectrally unmixing these pixels into proportional surface features, it is possible to extract valuable information from moderate spatial resolution imagery, to produce maps of ASM. Although legally permitted mineral concession areas have been delineated by the Peruvian government, the extent of mineral extraction within these areas, that is, the proportion of legal exploitation, has not been monitored, nor has the incidence of ASM outside of permitted concessions been mapped.

ASM in Madre de Dios has caused an estimated 320 km^2 (32,000 ha) of forest loss (Fraser 2009), with the rate of loss increasing from 292 ha/yr in 2006 to 1915 ha/yr in 2009, yielding a total estimate of 15,500 ha of ASM in 2009 (Swenson et al. 2011). ASM areas are spatially and spectrally distinct based on their proximity to stream channels and a high degree of exposed soil, in and around the associated ponds and tailings (Swenson et al. 2011). The Huepetuhe, Guacamayo and Delta-1 mining areas represent these characteristics and are easily detected, as they cover areas on the order of 100 km^2.
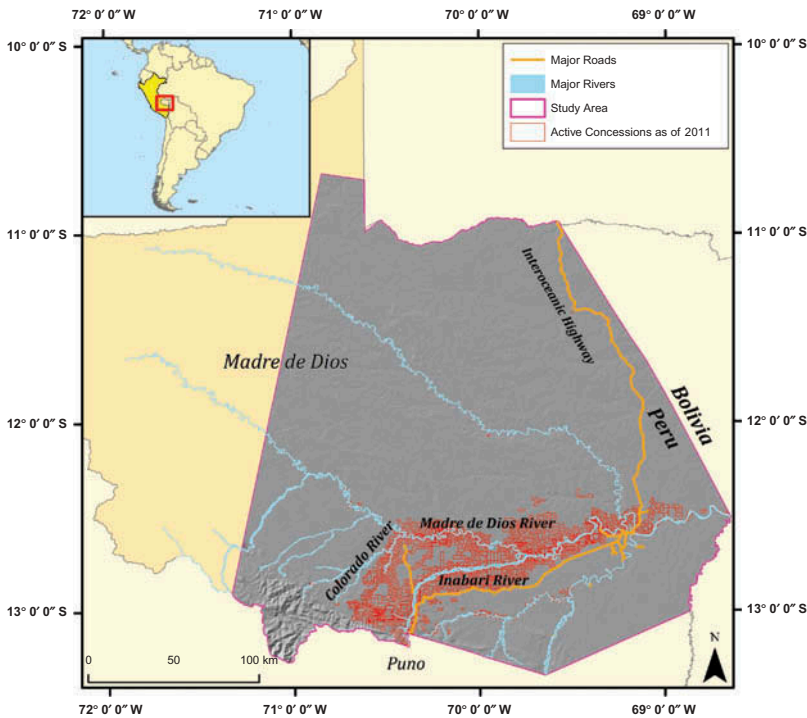
Figure 1. The location of the study area in Madre de Dios, Peru.

Conversely, many smaller ASM sites (<10 km^2) dot the study area. Asner et al. (2013) estimate approximately 45,000 ha of ASM in 2011, far more than the Swenson et al. (2011) estimate; this larger estimate reflects the increased detection rate of ASM using subpixel methods. The primary goal of this study is to further refine the detection of these small ASM locations and to assess their extent relative to legal mining concessions.

2. Study area

The study area is a 57,000 km^2 subset of the Madre de Dios Department of Peru (Figure 1). Both licit and illicit gold mining have been carried out in this region since the 1980s, with a rapid increase in ASM activity in the last decade (Asner et al. 2010, 2013; Swenson et al. 2011; Damonte et al. 2013). Although initially supported by the Peruvian government with legal concessions, much ASM is now carried out illegally, as focus has shifted to larger-scale mines operated with foreign investments (Damonte 2008, 135–74). Nevertheless, ASM has continued to expand, due to both the increase in international gold prices and the overall weakness of government in Madre de Dios (Swenson et al. 2011; Damonte 2014). Indeed, in Peru (Mosquera, Chávez, and Pachas 2009; Pachas 2011) and elsewhere (e.g. Hilson 2005), efforts to monitor ASM and foster its formalization have been hindered by limited government capacity and a more general inadequacy of knowledge regarding the composition and organization of the ASM sector.

For the purpose of this study, the Madre de Dios study area was defined by the intersection of four Landsat scenes and the Peru national border with Bolivia and Brazil, as indicated by Figure 1. Dominant vegetation comprises mostly tropical lowland rainforest with high biodiversity, and the area is one of the largest remaining uninterrupted

expanses of rainforest in the region (Swenson et al. 2011). Three major rivers, critical water supplies for ASM, cross the study area: the Madre de Dios from west to east and Colorado and Inambari from south to north. The study area is topographically flat, with a mean slope of 7% and a mean elevation of 330 m. The recently constructed Interoceanic Highway crosses through the southeastern portion of the region; this has helped spur deforestation for land development (Naughton-Treves 2004; Southworth et al. 2011).

3. Data

Landsat-5 TM imagery provided the primary data for this mapping project. The study area comprised tiles from path/row 2/68, 2/29, 3/68, 3/69, with imagery captured on 27 August 2011 and 3 September 2011. These image dates correspond to the mid-dry season (SENAMHI 2011), aiding in detection of ASM areas against the vegetation background. The imagery was downloaded from the USGS EarthExplorer website (http://earthexplorer. usgs.gov/) as pre-atmospherically corrected and radiometrically calibrated reflectance images and was then mosaicked and clipped to the study area boundaries. Ancillary data include active mining concession polygons for 2011 (http://geocatmin.ingemmet.gob.pe/geocatmin/), an ASTER 30-m digital elevation model and derived slope map, stream channel polygon data obtained from the Peruvian Ministry of the Environment (MINAM) Geoserver and a major roads polygon data-set. The streams and roads polygons were used to create distance rasters for the image classification process. Map validation relied on two fine spatial imagery data-sets comprising 17 individual tiles covering approximately 12,000 km^2, consisting of 2.5 m QuickBird and 2 m WorldView-2 multispectral, as well as 1 m WorldView-1 panchromatic imagery, acquired between August 2010 and August 2012 (DigitalGlobe 2010–2012).

4. Methods

4.1 Spectral mixture analysis

SMA was carried out on the Landsat-5 TM imagery to extract sub-pixel information of proportional coverage of each endmember class per pixel. SMA yields a set of images equal to the number of endmembers, plus one image showing residual values per pixel, indicating how well the combination of endmembers represents the pixel's actual reflectance values. Spectral unmixing was deemed to be acceptably accurate based on the overall low residuals throughout the study area (<0.05). Much of the residual error was deemed to be noise, with little geographic coherence, except along rivers, which showed some degree of clustered, comparatively high residual values.

The endmembers were selected based on contextual scene knowledge and trial-and-error iteration, ultimately yielding the following endmembers: photosynthetic vegetation, non-photosynthetic vegetation, water and three soil types, as shown Figure 2. The mineral composition of the soil endmembers is unknown; however, they are representative of the dominant soil signals in the imagery. The spectral responses of soil types 1 and 3 are similar in shape, differing mostly in magnitude, and conform to the iron-dominated reflectance curves of many soils (Hunt 1977). Soil type 2 is similar through bands 1 to 4, but shows a marked reflection decrease in the shortwave infrared bands, indicating either mineral-based or water-based absorption. ASM produces a somewhat heterogeneous land cover, consisting primarily of purification pools interspersed with exposed soil; overall, exposed soil and turbid water dominate the spectral response for these sites (Asner et al. 2013). The SMA process was iterated with different endmembers and different endmember training pixels until the overall residuals image showed residual values no greater than 0.05.
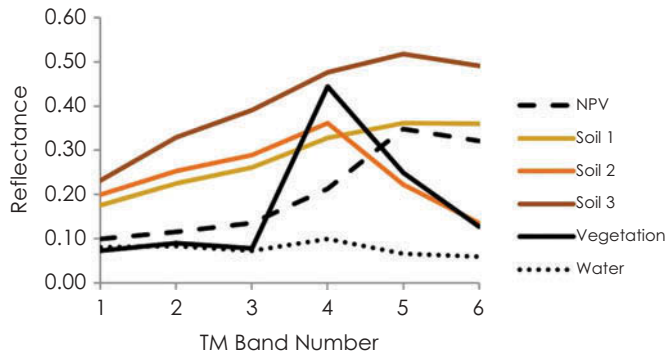
Figure 2.   Endmember spectral signatures used to unmix Landsat imagery in this study.

4.2 Image classification

CTA was carried out using the six fraction images, as well as the elevation, slope, distance to rivers and distance to roads images. The CTA used the Gini splitting rule, which maximizes node purity (Zambon et al. 2006). Five categories were used for the final classification: ASM, water, agriculture, forest and natural alluvial deposits. A 3 × 3 mode filter was used on the land-cover map to reduce speckle caused by topographic and other shading influences.

4.3 Active concessions overlay

The extent of licit mineral exploration was determined by overlaying the ASM classification map with a polygon data-set of active mining concession areas. Locations within the study area that did not fall within the active concessions polygon were deemed 'illicit', while those within were deemed 'licit' (Cuba et al. 2014).

4.4 Map validation

QuickBird, WorldView-1 and WorldView-2 imagery were used to validate the Landsat-derived land-cover map. This imagery was acquired for a coincident time period, with panchromatic and multispectral images from August 2010 to August 2012. A categorically and spatially stratified sampling design used 580 validation points that were randomly generated within the study region, with a minimum of 50 points per land-cover category. Further, the points were constrained to a 2 km buffer of stream channels, in order to avoid a spuriously inflated accuracy estimate caused by the forest class, which is both the most abundant and the most spectrally distinct. This spatial stratification relies on the observation that ASM activities require proximity to a major water source for operation (Cuba et al. 2014). For each validation point, the true land cover was ascertained by manual interpretation of the fine spatial resolution imagery. The mapped and true cover was then cross-tabulated for accuracy assessment, yielding commission error, omission error and overall accuracy, shown in Table 3. Because the distribution of reference samples per category was not proportional to the area of that category in the map, the per-category accuracies were weighted based on their areal proportion to calculate the overall accuracy. For example, since forest class dominates the study area, its relative contribution to overall accuracy is much higher than agriculture, which covers much less area.

5.   Results

Based on the reference imagery, the overall area-weighted map accuracy was 96% (87% raw overall accuracy) (Table 3). The omission error for ASM was 29%, and the commission error was 31%. Classification tree results showed primary decision splits for the distance-to-rivers, proportion vegetation and proportion water, indicating that these variables most clearly separate the target categories. All input variables contributed to the classification tree, with elevation being least important. For the entire study area, 65,000 ha were mapped as ASM, with 23,000 ha falling within active concessions (Table 1). This shows that 36% of all ASM area falls within the active legal mineral extraction concessions. The classification error matrix is shown in Table 2. Classification confusion exists between ASM and natural alluvium and also between alluvium and river categories.

Three previously mapped areas of larger-scale mining – Huepetuhe, Guacamayo and Delta-1 (Swenson et al. 2011; Asner et al. 2013) – were detected successfully (Figure 3). The more numerous smaller extent (>10 km^2) ASM locations were also detected successfully (Figure 4), based on validation using interpretation of the fine-resolution imagery.

6.   Discussion and conclusions

Mapping ASM locations with Landsat imagery is challenging due to their small areal extent and spectral similarity to natural alluvial features. The combination of SMA and CTA methods presented here sought to overcome these challenges by extracting physically based land-cover proportions and invoking ancillary data for physical context. These methods produced plausible results, based on the random sampling validation and also a holistic visual interpretation of the CTA map with the fine spatial resolution data, shown in Figure 4. The large, previously documented mining areas are seen clearly in Figure 3 and exhibit a

Table 1.   Land use category areal extents (ha) inside and outside of mining concessions as of 2011.

		Land-cover class					
		Forest	Agriculture	ASM	Alluvium	River	Total
Mining concession status	**Entire study area**	5,493,000 96.1%	79,400 1.4%	65,100 1.1%	50,500 0.9%	25,200 0.4%	5,713,300 100%
	No concession	5,084,300 97.1%	68,400 1.3%	41,800 0.8%	33,000 0.6%	11,300 0.2%	5,238,700 100%
	Active concession	408,700 86.1%	11,000 2.3%	23,400 4.9%	17,500 3.7%	13,900 2.9%	474,500 100%

Table 2.   Accuracy assessment cross tabulation, based on the classification output (rows) and the fine resolution reference imagery (columns).

		Reference image					
		Forest	Agriculture	ASM	Alluvium	River	Total
Classification output	**Forest**	321	1	4	4	2	**332**
	Agriculture	10	33	5	3	0	**51**
	ASM	1	4	24	2	3	**34**
	Alluvium	0	5	1	41	15	**62**
	River	0	0	1	4	20	**25**
	Total	**332**	**43**	**35**	**54**	**40**	**504**
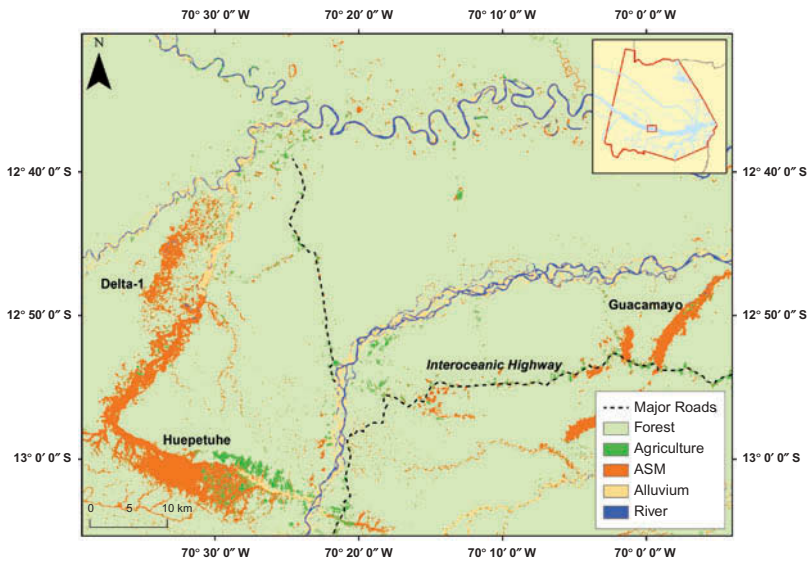
Figure 3.   Final CTA output showing three previously documented mining locations: Huepetuhe, Guacamayo and Delta-1.
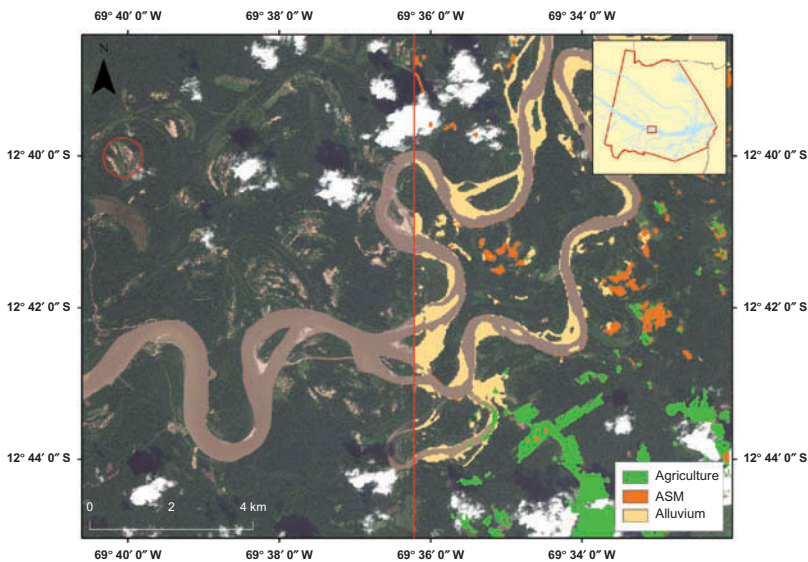
Figure 4.   Enhanced image of artisanal small-scale Mining and agriculture areas along the Madre de Dios River. The eastern portion of the figure shows ASM, agriculture and natural alluvium, overlaid with QuickBird imagery, while the western portion shows only the imagery, with a ring around a typical ASM location.

heterogeneous pattern caused by interspersed agriculture, non-ASM soil and water, and what appear to be abandoned older mines. Compared to a previous ASM map produced by Swenson et al. (2011), the Guacamayo site appears to have extended southwards across the newly constructed Interoceanic Highway; this extension is excluded from legal concession areas, as illustrated in Figure 5, and is an example of illicit mining activity. Numerous small

patches of ASM are visible along the Madre de Dios River. These locations are spatially coherent and appear to be well classified, based on comparison to the QuickBird imagery shown in Figure 4. Overall, 65,129 ha of ASM was predicted for the study area, considerably larger than the 15,500 ha predicted by Swenson et al. (2011). This discrepancy is likely due to the improved detection of small ASM patches using the proposed SMA/CTA methods and also due to the temporal offset between the two studies. Asner et al. (2013) reported roughly 45,000 ha of forest to ASM conversion in Madre de Dios by 2011, and while this estimate is much closer to that presented here, the study area extent used by Asner et al. was more limited.

The distance-to-rivers and distance-to-roads variables were particularly useful for discriminating ASM from natural alluvium, as ASM typically occurs in intentionally remote and obscured locations, but also requires access to water and transportation. These small, clandestine ASM locations are the primary target for this mapping effort, since the Huepetuhe, Guacamayo and Delta-1 mining locations are plainly visible in Landsat imagery and can easily be classified with more traditional methods. As shown in Figures 4 and 5, ASM locations are typically associated with small-scale agriculture activities, also discriminated from other spectrally similar classes on the basis of their distance from rivers and roads. ASM/alluvium confusion is problematic for parts of the scene, most likely due to the similar spectral responses of the soil exposed by mining and that exposed by natural erosion processes. These categories were separated fairly well based on the distance-to-rivers variable, since ASM locations tend to be slightly farther away from rivers; however, this decision rule did not perfectly distinguish all cases of these two land-uses. Alluvium/water confusion also reduced overall accuracy and was likely caused by shallow water with a high spectral contribution from the underlying river sediment or by ephemeral streams and seasonal river depth changes associated with precipitation.

Some degree of classification confusion between ASM and other categories was caused by the mismatch in spatial resolution of the output map (30 m) and the validation imagery (~0.5 to 2.5 m); this mismatch is particularly relevant for validation points falling close to the edge of a landscape patch or ASM area. Such points potentially introduce spurious errors due to the nature of hard classification of inherently mixed pixels. Therefore, the accuracy estimates provided in Tables 2 and 3 may be overly pessimistic.

ASM activity is not well confined by legal mining concessions in Madre de Dios, as illustrated in Figure 5, which shows active mining concessions. This image is centred on the southern expansion of the Guacamayo mining area and shows the expansion of licit operations into new, illicit areas. This figure also shows smaller-scale mining occurring outside but adjacent to legal concessions, in this case along the Malinowski River in the southern portion of the map. In total, 64% of mapped ASM occurs in areas with no active mining concessions. Even allowing for commission error of ASM, the proportion of illicit mining is very high in the study area, with 64% of ASM occurring in non-concession areas.

Due to the logistical difficulties of *in situ* monitoring of illicit mining activities in the remote Madre de Dios region, Landsat imagery, together with other free, publically

Table 3. Accuracy report for classification.

Class	Omission Error	Commission Error	Overall Accuracy
Forest	3.31%	3.31%	**95.6%**
Agriculture	23.26%	35.29%	
ASM	31.43%	29.41%	
Alluvium	24.07%	33.87%	
River	50%	20%	

Note: The overall accuracy figure accounts for the relative abundance of each land use type in the study area.
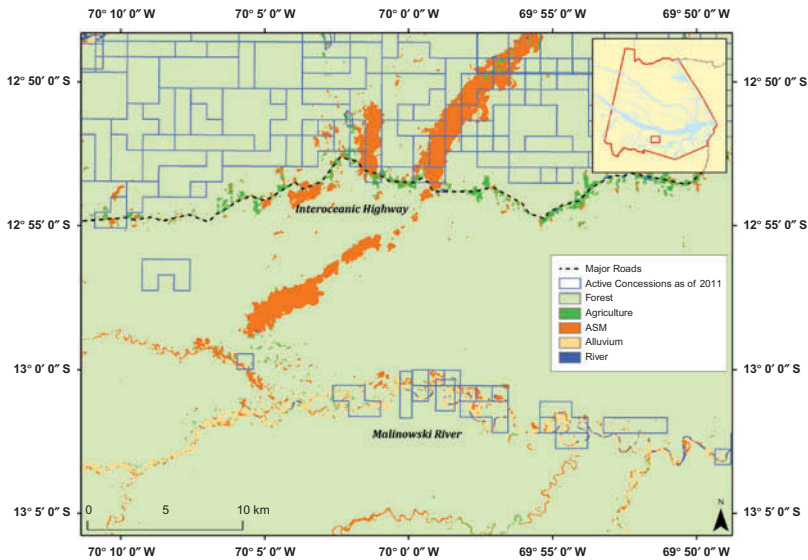
Figure 5. Classification tree output, showing active mineral extraction concessions in 2011. Note that a large proportion of the ASM activity falls outside of these concessions.

available ancillary data-sets, presents a practical and effective alternative. The use of SMA and CTA for this classification proved to be effective based on validation using fine spatial resolution imagery. Furthermore, the small patches of ASM located in the output classification are consistent with the type of mining that is occurring in this region, as shown by previous research (e.g. Asner et al. 2013) and by the fire resolution imagery. As these methods rely on free, easily accessible data and straightforward methods, it is reasonable to assume that they could successfully be implemented in other areas experiencing similar ASM activity. Future research will explore this possibility, as well as the potential for expanding temporal coverage using Landsat-8 imagery.

References

Asner, G. P., W. Llactayo, R. Tupayachi, and E. R. Luna. 2013. "Elevated Rates of Gold Mining in the Amazon Revealed through High-Resolution Monitoring." *Proceedings of the National Academy of Sciences* 110 (46): 18454–18459. doi:10.1073/pnas.1318271110.

Asner, G. P., G. V. N. Powell, J. Mascaro, D. E. Knapp, J. K. Clark, J. Jacobson, T. Kennedy-Bowdoin, A. Balaji, G. Paez-Acosta, E. Victoria, L. Secada, M. Valqui, and R. F. Hughes. 2010. "High-Resolution Forest Carbon Stocks and Emissions in the Amazon." *Proceedings of the National Academy of Sciences* 107 (38): 16738–16742. doi:10.1073/pnas.1004875107.

Baynard, C. W. 2011. "The Landscape Infrastructure Footprint of Oil Development: Venezuela's Heavy Oil Belt." *Ecological Indicators* 11 (3): 789–810. doi:10.1016/j.ecolind.2010.10.005.

Baynard, C. W., J. M. Ellis, and H. Davis. 2013. "Roads, Petroleum and Accessibility: The Case of Eastern Ecuador." *GeoJournal* 78 (4): 675–695. doi:10.1007/s10708-012-9459-5.

Bebbington, A., D. H. Bebbington, J. Bury, J. Lingan, J. P. Muñoz, and M. Scurrah. 2008. "Mining and Social Movements: Struggles over Livelihood and Rural Territorial Development in the Andes." *World Development* 36 (12): 2888–2905. doi:10.1016/j.worlddev.2007.11.016.

Brooks, W. E., E. Sandoval, M. A. Yepez, and H. Howard. 2007. *Peru Mercury Inventory 2006*. Reston, VA: US Geological Survey.

Cuba, N., A. Bebbington, J. Rogan, and M. Millones. 2014. "Extractive Industries, Livelihoods and Natural Resource Competition: Mapping Overlapping Claims in Peru and Ghana." *Applied Geography*. doi:10.1016/j.apgeog.2014.05.003.

Damonte, G. 2008. *The Constitution of Political Actors: Peasant Communities, Mining, and Mobilization in Bolivian and Peruvian Andes*. Saarbrücken-Berlin: VDM Publishing.

Damonte, G. 2014. "Playing at the Margins of the State: Small Scale Miners and the State Formalizing Quest in Madre de Dios." In *Latin American Studies Association Conference*, Chicago, IL: GOMIAM, Small Scale Gold Mining in the Amazon.

Damonte, G., M. B. de Mesquita, V. H. Pachas, M. C. Quijada, A. Flores, and J. de Echave Cáceres. 2013. "Small-Scale Gold Mining and Social and Environmental Conflict in the Peruvian Amazon." In *Small-Scale Gold Mining in the Amazon*, edited by L. Cremers, J. Kolen, and M. de Theije, 68–84. Amsterdam: CEDLA.

DigitalGlobe. 2010–2012. *Quickbird Multispectral and Worldview-1 and Worldview-2 Panchromatic Scenes, Level Standard 2A*. Longmont, CO. www.digitalglobe.com

Erener, A. 2011. "Remote Sensing of Vegetation Health for Reclaimed Areas of Seyitömer Open Cast Coal Mine." *International Journal of Coal Geology* 86 (1): 20–26. doi:10.1016/j.coal.2010.12.009.

Fraser, B. 2009. "Peruvian Gold Rush Threatens Health and the Environment." *Environmental Science & Technology* 43 (19): 7162–7164. doi:10.1021/es902347z.

Gardner, E. 2012. "Peru Battles the Golden Curse of Madre de Dios." *Nature* 486 (7403): 306–307. doi:10.1038/486306a.

Hentschel, T., F. Hruschka, and M. Priester. 2002. "Global Report on Artisanal and Small Scale Mining." Report commissioned by the Mining, Minerals and Sustainable Development of the International Institute for Environment and Development. Download from http://www.iied.org/mmsd/mmsd_pdfs/asm_global_report_draft_jan02.pdf

Hilson, G. 2002. "An Overview of Land Use Conflicts in Mining Communities." *Land Use Policy* 19 (1): 65–73. doi:10.1016/S0264-8377(01)00043-6.

Hilson, G. 2005. "Strengthening Artisanal Mining Research and Policy through Baseline Census Activities." *Natural Resources Forum* 29 (2): 144–153.

Hunt, G. R. 1977. "Spectral Signatures of Particulate Minerals in the Visible and near Infrared." *Geophysics* 42 (3): 501–513.

Latifovic, R., K. Fytas, J. Chen, and J. Paraszczak. 2005. "Assessing Land Cover Change Resulting from Large Surface Mining Development." *International Journal of Applied Earth Observation and Geoinformation* 7 (1): 29–48. doi:10.1016/j.jag.2004.11.003.

Mosquera, C., M. Chávez, and V. Pachas. 2009. *Estudio Diagnóstico De La Actividad Minera Artesanal En Madre de Dios*. Lima: Fundación Conservación Internacional.

Naughton-Treves, L. 2004. "Deforestation and Carbon Emissions at Tropical Frontiers: A Case Study from the Peruvian Amazon." *World Development* 32 (1): 173–190. doi:10.1016/j.worlddev.2003.06.014.

Pachas, V. 2011. *A Propósito Del Plan Nacional Para La Formalización De La Minería Artesanal En El Perú*. Lima: CooperAcción.

SENAMHI (Servico Nacional de Meteorología e Hidrología del Perú). 2011. "Guía Climática Turística." http://www.senamhi.gob.pe/main_down.php?ub=est&id=guia_GuiaClimaticaTuristica.

Slonecker, T., G. B. Fisher, D. P. Aiello, and B. Haack. 2010. "Visible and Infrared Remote Imaging of Hazardous Waste: A Review." *Remote Sensing* 2 (11): 2474–2508. doi:10.3390/rs2112474.

Southworth, J., M. Marsik, Y. Qiu, S. Perz, G. Cumming, F. Stevens, K. Rocha, A. Duchelle, and G. Barnes. 2011. "Roads as Drivers of Change: Trajectories across the Tri-National Frontier in MAP, the Southwestern Amazon." *Remote Sensing* 3 (5): 1047–1066. doi:10.3390/rs3051047.

Swenson, J. J., C. E. Carter, J.-C. Domec, and C. I. Delgado. 2011. "Gold Mining in the Peruvian Amazon: Global Prices, Deforestation, and Mercury Imports." *Plos One* 6 (4): e18875. doi:10.1371/journal.pone.0018875.

Vásquez Cordano, A. L., and E. J. Balistreri. 2010. "The Marginal Cost of Public Funds of Mineral and Energy Taxes in Peru." *Resources Policy* 35 (4): 257–264. doi:10.1016/j.resourpol.2010.08.002.

Veiga, M. M., P. A. Maxson, and L. D. Hylander. 2006. "Origin and Consumption of Mercury in Small-Scale Gold Mining." *Journal of Cleaner Production* 14 (3–4): 436–447. doi:10.1016/j.jclepro.2004.08.010.

Yard, E. E., J. Horton, J. G. Schier, K. Caldwell, C. Sanchez, L. Lewis, and C. Gastañaga. 2012. "Mercury Exposure among Artisanal Gold Miners in Madre de Dios, Peru: A Cross-Sectional Study." *Journal of Medical Toxicology* 8 (4): 441–448. doi:10.1007/s13181-012-0252-0.

Zambon, M., R. Lawrence, A. Bunn, and S. Powell. 2006. "Effect of Alternative Splitting Rules on Image Processing Using Classification Tree Analysis." *Photogrammetric Engineering and Remote Sensing* 72 (1): 25–30. doi:10.14358/PERS.72.1.25.